

Radiation Physics and Engineering 2021; 2(1):9–17

<https://doi.org/10.22034/rpe.2021.252856.1026>

Feasibility study of Mo-99 production using high-power electron Linac: Nuclear and thermal-mechanical analysis based on photoneutron interaction

Ali Taghibi Khotbeh-Sara^a, Faezeh Rahmani^{a,*}, Farshad Ghasemi^b

^aDepartment of Physics, K.N. Toosi University of Technology, Tehran, Iran

^bNuclear Science and Technology Research Institute (NSTRI), Tehran, Iran

HIGHLIGHTS

- Target design for an accelerator-based method for Mo-99 production.
- Investigation on one-stage and two-stage methods using photoneutron in Mo-100.
- Target design using nuclear simulation by MCNPX2.6 and thermal analysis by COMSOL.
- Suggested conceptual design of the target includes nine Mo-100 stripe plates and cooling system.

ABSTRACT

This work presents an alternative method for Mo-99 production as a parent nuclide of Tc-99m which is the most used radioisotope in diagnostic imaging processes. Regarding to some benefits of accelerator-based methods over reactor-based methods for Mo-99 production, the electron Linac-based method has been selected. In this way of production, two approaches (one-stage and two-stage) are available using photoneutron reaction in Mo-100 target using bremsstrahlung photons. The superiority of one-stage approach and optimal dimension of target has been demonstrated by nuclear simulation using MCNPX2.6 code. Thermal analysis of the optimized target has been performed by COMSOL software, which has been led to select the indirect cooling system. The final suggested conceptual design of the target includes nine Mo-100 stripe plates with 0.2, 3, and 30 cm in thickness, width and length, respectively which being surrounded by two copper clamps as the cooling ducts. The velocity of 2.5 m/s of inlet coolant (water) is sufficient for the suggested cooling system to satisfy the conditions of the turbulent regime as the desired cooling regime.

KEYWORDS

Mo-99 production
Electron linear accelerator
Photoneutron
Monte Carlo MCNPX2.6 code
COMSOL

HISTORY

Received: 10 September 2020
Revised: 21 November 2020
Accepted: 24 November 2020
Published: January 2021

1 Introduction

The most widely used diagnostic radioisotope in the clinical practice of nuclear medicine is Tc-99m, which covers 35 million diagnostic imaging processes annually (Peykov and Cameron, 2014). 140 keV single-gamma emission, which is proper for imaging, short half-life (about 6 h) with the decrease in patient's received dose and subsequently radiation side effects, and also the capability of combination with various carriers appropriate for different organs, are the reasons of the widespread use of Tc-99m. Because Tc-99m has a short half-life, Mo-99 (transforms into Tc-99m in β decay mode ($t_{1/2} = 66$ h)) is also produced as a desirable option.

The research study on Mo-99 isotope supplies has been

reported by the American Medical Isotopes Production Act of 2012 (AMIPA) in 2016, which shows most of the global supply (about 95%) of Mo-99 for medical use is produced in seven research reactors (by irradiating uranium targets) located in Australia, Canada, Europe, and South Africa. The remainder (about 5%) of the global supply is produced for regional use in other countries (National Academies of Sciences et al., 2016).

Two major reactor-based methods are: (1) the processing of fission products of U-235 target (about 6.1% of the fissions leads to Mo-99 production) and (2) the neutron activation of Mo-98 target (through the neutron capture reaction) (National Academies of Sciences et al., 2016). Some shortcomings of reactor-based methods are: (1) shut down of the reactor (suddenly accidents, predetermined

*Corresponding author: frahmani@kntu.ac.ir

repairing programs or expired operating life), (2) unavoidable production of undesirable isotopes in products (with the need to expensive separation process), and (3) the need to HEU (high-enriched uranium) with more cost and safety challenges to achieve Mo-99 with high activity (National Academies of Sciences et al., 2016; Tsechanski et al., 2016; Ross et al., 2010; Council et al., 2009). So, the alternative production methods as a short, middle or long-term solution are necessary. According to this demand, different researches have been followed for Mo-99/Tc-99m production using non-reactor methods (Council et al., 2009; Bradley, 2013; Esposito et al., 2017; Junior, 2017; Esposito et al., 2013; IAEA, 2017; Fong et al., 2008).

Accelerator-based production is an alternative method for direct Tc-99m production using cyclotron ($^{100}\text{Mo}(p,2n)^{99m}\text{Tc}$) or Mo-99 production using high power electron linear accelerator (Linac) via $^{100}\text{Mo}(\gamma,n)^{99}\text{Mo}$. Cyclotron-based method has a significant production yield (JANIS, 2020a; Rovais et al., 2016), but it may be limited in application due to the short half-life of Tc-99m.

On the other hands, Linac-based method can be an appropriate method due to Mo-99 production as well as according to the safety and economic aspects (Ross and Diamond, 2015; Diamond et al., 2017). Two main approaches, one-stage and two-stage approaches can be followed using Linac. In two-stage approach, the electron beam is converted to high-energy bremsstrahlung photons in the high-density high-Z target (such as W or Ta), then Mo-99 is produced via photoneutron reactions with energetic photons (energy more than the threshold of photoneutron reaction) in the Mo-100 target (Diamond et al., 2018). The description of the designed system by Canadian Light Source (CLS) can be found in the related reference (Diamond et al., 2018).

In one-stage approach as a novel method (Tsechanski et al., 2016), a target is electron-photon converter as well as the photoneutron target simultaneously, so self-absorption of photons in electron-photon converter can be prevented and produced photons can participate directly in photoneutron reactions, which results the increases in the production yield of Mo-99 (Tsechanski et al., 2016). Argonne National Laboratory has conducted several demonstrations of the technology in collaboration with Los Alamos National Laboratory and proved the feasibility of this approach (Dale et al., 2010; Fedorchenko and Tsechanski, 2019) to produce activity of 190 Ci per day using 33 MeV electron beam (120 kW) (Dale et al., 2012).

In the present work, two above mentioned approaches with different designs of Mo-100 target have been discussed based on Linac (photoneutron reaction) to obtain the optimized target for Mo-99 production using MCNPX2.6 Monte Carlo Code (Pelowitz, 2008). Beside the nuclear aspects in designing the target, thermal-mechanical aspects should be also considered. Therefore, cooling the target assembly with appropriate coolant and applying proper conditions play a vital role in the target design. In this work, thermal analysis of target has been performed using COMSOL software (COMSOL, 2011).

According to these, the conceptual design of the target has been presented by considering nuclear-mechanical features.

2 Materials and methods

The conceptual design of Mo-100 target including nuclear calculation and thermal analysis has been performed using MCNPX2.6 code and COMSOL software, respectively and the final design has been redesigned for working in real conditions.

The first requirement to produce Mo-99 isotope through to the bremsstrahlung and subsequently photoneutron reaction in the Mo-100 is to provide an appropriate electron source such as Linac. The energy as well as the current of electron beam is the main effective parameters. Through bremsstrahlung interaction in Mo-100, photons with continues spectrum (low energy up to endpoint energy equal to maximum electron energy) are produced. The threshold energy and maximum cross section of the photoneutron reaction in Mo-100 is about 9 and 14 MeV, respectively (JANIS, 2020b). According to the relation between the produced bremsstrahlung spectrum and electron energy, high-energy electron beam between 25 and 45 MeV is needed. Fortunately, technology of the high-energy industrial Linacs are available in recent years (Brown, 2014) Linac with 30 MeV in energy and (1 mA in current) has been selected. So, the calculations of upcoming results have been performed based on 30 MeV continues electron beam with 1 mA in current. Although the increase in electron energy up to 45 MeV increases the production rate of photon, but the unwanted reaction channels with high energy photons and photoneutrons will produce undesired isotopes and particles as well (Bennett et al., 1999). It should be noted that the average relative errors of MCNPX2.6 Monte Carlo results are less than 5%.

3 Target design in two-stage approach

The two-stage approach, as described above, is a more general and earlier method, which uses two separate targets. At first, high-density high-Z target such as tungsten is used to produce high-energy photons. It should be noted that other high-density high-Z targets (such as tantalum, uranium, rhenium, etc.) can be also used as an electron-photon converter (Torabi et al., 2013); but tungsten with higher melting point, better thermal conductivity and easy to access can be an appropriate choice. Figure 1 shows the comparison between tungsten and tantalum photon production yield (in the same saturated radius of 0.4 cm). As Fig. 1 shows, it is important to calculate the yield of high-energy photons with energy more than 9 MeV according to threshold energy of photon for photoneutron production (Fig. 2), which are effective in Mo-99 production. Therefore, to achieve the highest effective photon flux, the optimized thickness of the converter should be determined.

In the next step, photons with energy more than threshold energy of photoneutron reaction in Mo-100 target leading to Mo-99 production has been calculated.

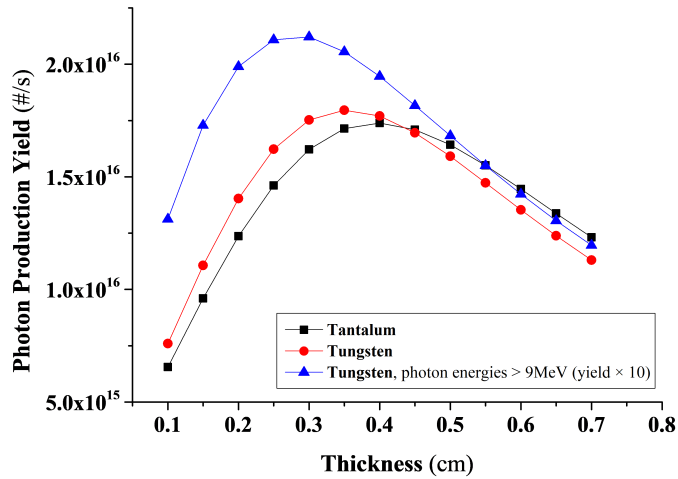


Figure 1: Comparison of the photon yield for W and Ta in the same radius of 4 mm.

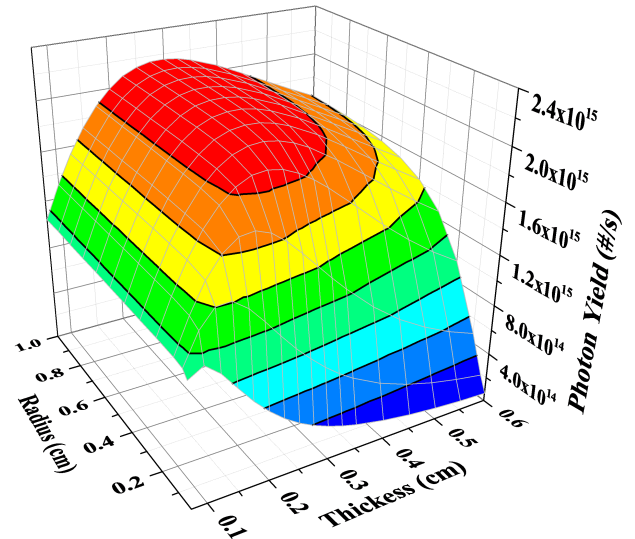


Figure 4: Photon yield in the tungsten (electron-photon converter target).

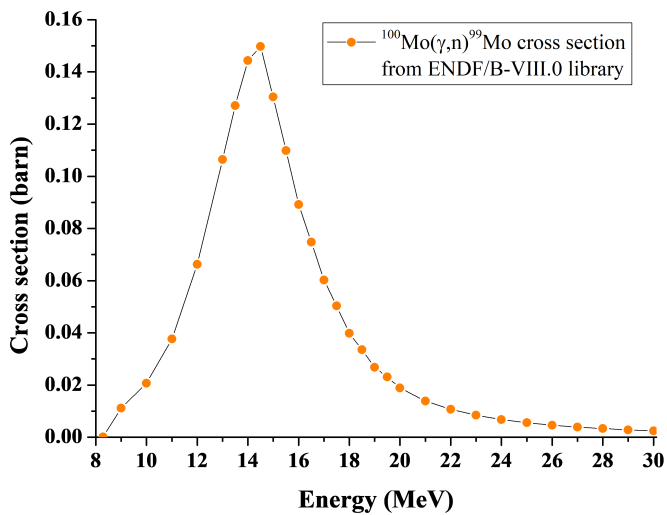


Figure 2: Cross section of Mo-99 production through photon-neutron interaction in Mo-100 target.

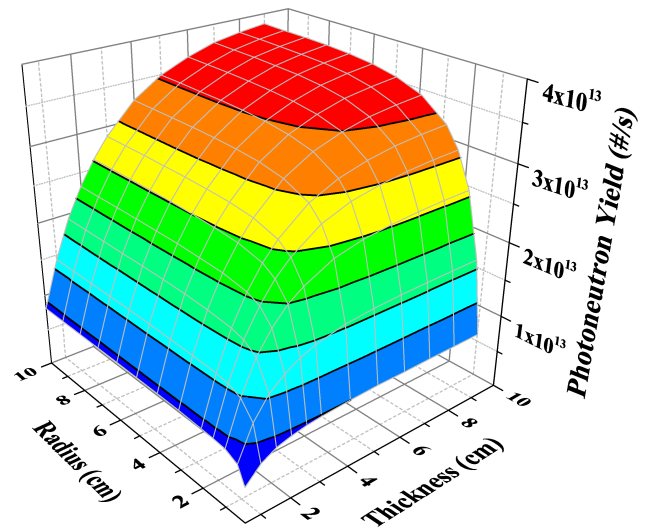


Figure 5: Photon-neutron yield (equivalent to Mo-99 production) in a Mo-100 cylindrical target.

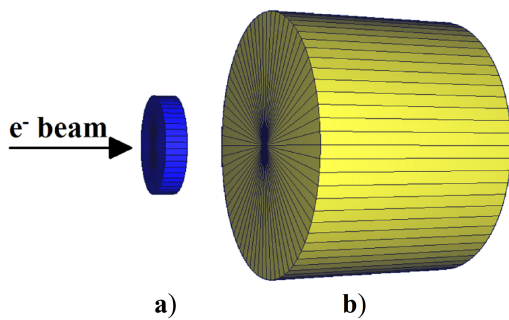


Figure 3: Schematic view of target geometry a) electron-photon converter target, b) Mo-100 target.

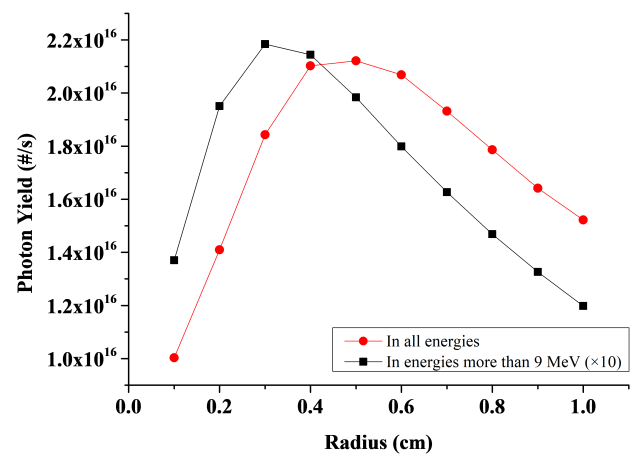


Figure 6: Photon yield in hemispherical tungsten converter (electron beam is incident on the convex side of hemisphere).

The geometries considered for the targets is shown in Fig. 3. The photon yield in the exit face of converter has been calculated for various dimensions of the tungsten disc by considering photon energies more than 9 MeV (Fig. 3) and then, photoneutron production rate (equivalent to Mo-99 production rate) has been calculated for the molybdenum cylindrical target (Fig. 5).

According to the results, the increase in radius more than 0.4 cm shows the increase of production yield less than 1% (stated as a saturated radius) in tungsten. For this saturated radius, the optimum thickness is about 0.3 cm. The optimized dimension of Mo-100 target has been calculated based on the criterion of minimum volume. Concerning cooling requirements, a distance of 1 cm has been assumed between W converter and Mo-100 target. Based on the simulation results (Fig. 5), by increasing the radius and thickness, the production efficiency of photoneutron yield is increased as well.

Bremsstrahlung photons have peak forward behavior, so large fraction of photons will be in the limited conical shape area (Diamond et al., 2017; Tsechanski et al., 2016). Therefore, among the different geometries for converter, a semi-spherical tungsten converter has been proposed as shown in Fig. 6. The optimum radius of hemispherical converter by considering photons with energy more than 9 MeV is approximately 0.3 cm. In larger radii, the population of photons is reduced due to the self-absorption in target. As shown in Fig. 10-a, 30 MeV electron beam is incident on the convex side of hemispherical target.

In real conditions, incidence of high power electron beam on the target can lead the local melting, so it is necessary to provide a solution for an appropriate heat removal problem. There are some solutions such as the use of the powerful coolant system, a radiation-cooled rotating target or immersed rotary target disc in water. Also, considering a long target with sweeping beam on the target in straight line will be useful. Besides all these issues, the distance between the converter and photoneutron target to embed the cooling system should be as small as possible to maximize entrance of photons from photon target into photoneutron target.

4 Target design in one-stage approach

Molybdenum is a high-density high-Z metal that can be used as an electron-photon converter. Photon flux of molybdenum is not quite as high as the produced photon in tungsten, however prevention of photon self-absorption is an advantage that made it desirable to use as the electron-photon converter as well as photoneutron target, for isotope production, simultaneously.

Figures 7 to 9 show the distribution of particles' population (electron, photon and neutron) as well as deposition of their energy in the volume of the massive cylindrical target. The peak forward bremsstrahlung photons are in the limited conical shape area, so relative to electrons direction, these photons are rarely in the angles of 0, 90, and 180 degrees and photon population are minimum in these areas (as shown in Fig. 8).

According to these results, the considerable volume

of target is useless and without significant production. Thus, based on the design from (Torabi et al., 2013) that suggested hemispherical geometry for converter, it has been decided to propose the new hemispherical designs as shown in Fig. 10.

As seen, the minor superiority of the hemispherical geometry can be seen in large dimensions. Also, when the electron beam incidents on the convex side of hemispherical target (Fig. 10-a), the expected yield will be a little more than another designs. The photon yields of molybdenum cylindrical target in various dimensions have been investigated as shown in Fig. 11. As seen, it is comparable with the result of W converter in Fig. 4.

Also, neutron production yield, which is equivalent to production rate of Mo-99, has been calculated in Mo-100 target with different volumes. The related results are shown in Figs. 12 and 13.

Figure 13 shows a comparison between neutron yields of hemispherical geometries and cylindrical geometry with two different thicknesses (7 and 3 cm, respectively as the saturated and middle case of Fig. 12) in corresponding with one-stage approach.

Also, a comparison between Figs. 5, 12, and 13) illustrates the superiority of one-stage approach over two-stage approach. If the neutron yield about 3.8×10^{13} n/s is considered as the saturate yield, the needed volume to reach the saturated yield in one-stage approach (radius of 3 cm, thickness of 7 cm and volume of 198 cm^3) is only about 6% of the needed volume in the same way in two-stage approach (radius and thickness of 10 cm and volume of 3141 cm^3).

Although the result of hemispherical target looks better according to nuclear calculations, considering the heat removal requirements, cylindrical target has been selected.

As mentioned previously, the deposited heat should be removed using cooling system, so it has been suggested to divide target into nine similar discs with 1 mm distance between them for cooling.

Since the scanning electron beam system is used, so the discs along each other can be considered as a long strip (Fig. 14-a). The proposed design is shown in Fig. 14-b, which includes nine Mo-100 strips with 3 cm in width and 2 mm in thickness as well as two copper tubes in both sides of plates for water-cooling. The length of target has been calculated in next section.

5 Design of cooling system

Cooling requirements is one of the main important challenges in target design. The deposited energy in the target has been calculated by MCNPX2.6 code, and thermal and mechanical analysis has been performed using finite element method by COMSOL Multiphysics (in steady-state thermal model).

Water and helium gas are used as a conventional coolant in this type of systems (Diamond et al., 2017). The water-cooling system is more economical, but due to the water corrosive effects, direct contact of water and target should be avoided. So, copper tube can be used as coolant channel, also as a holder for target structure.

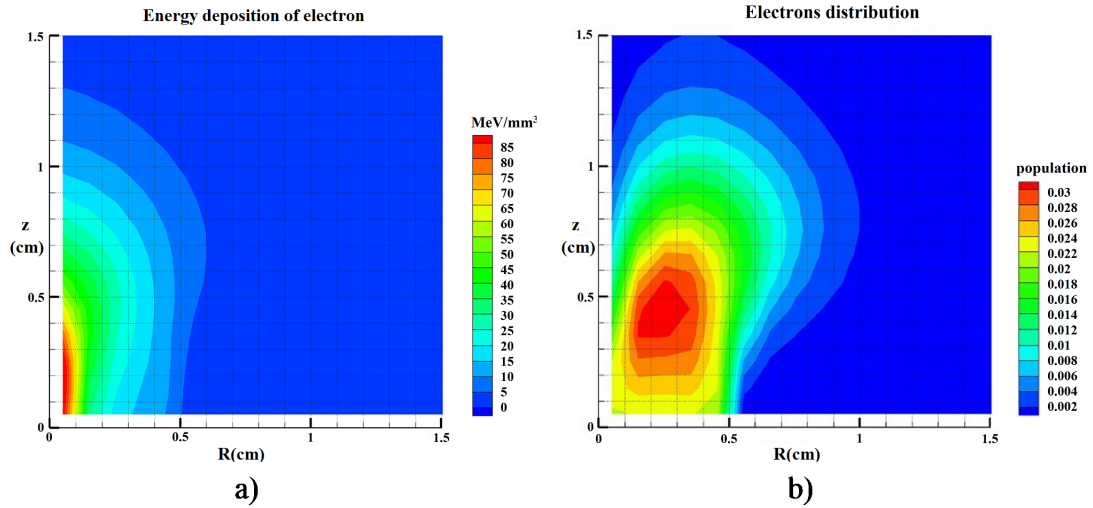


Figure 7: 2D cross-sectional images of a) average energy deposition of electron and b) spatial distribution of electrons, per unit volume of each mesh (1 mm^3) and one source particle. (The radius of e-beam is 0.5 cm).

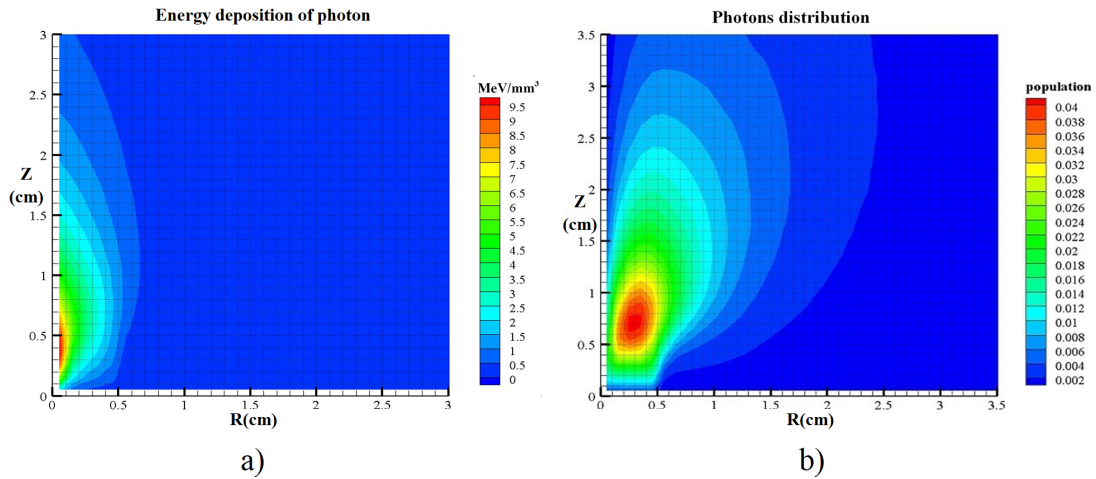


Figure 8: 2D cross-sectional images of a) average energy deposition of photon and b) spatial distribution of photons, per unit volume of each mesh (1 mm^3) and one source particle. (The radius of e-beam is 0.5 cm).

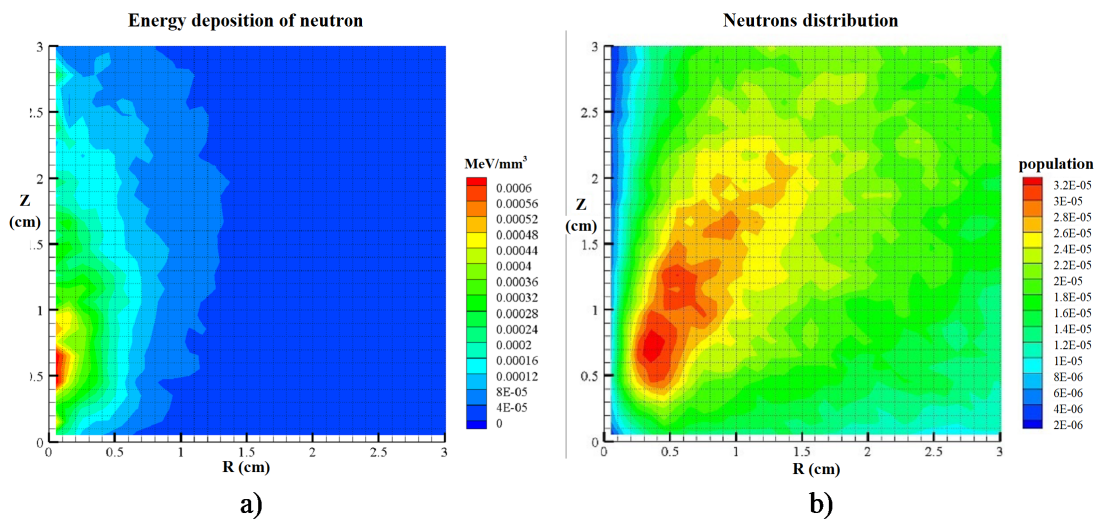


Figure 9: 2D cross-sectional images of a) average energy deposition of neutron and b) spatial distribution of neutrons, per unit volume of each mesh (1 mm^3) and one source particle. (The radius of e-beam is 0.5 cm).

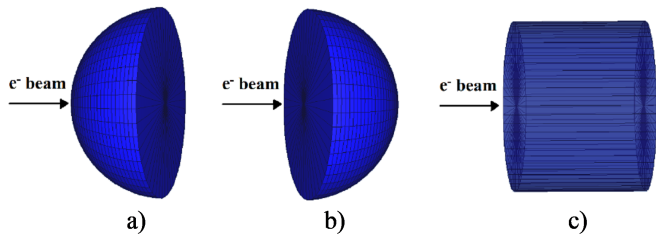


Figure 10: Suggested Mo-100 target geometries for one-stage approach: a) semispherical (electron beam incidents on convex side), b) hemispherical (electron beam incidence on flat side), c) cylindrical.

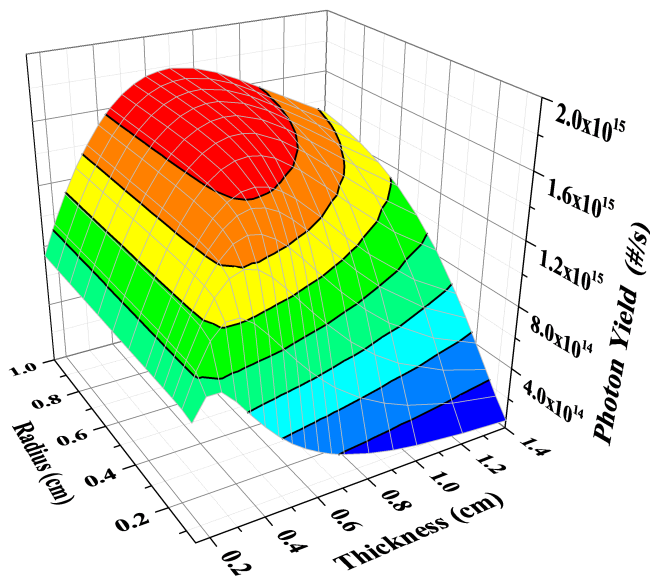


Figure 11: Yield of the bremsstrahlung photons in cylindrical Mo-100 target.

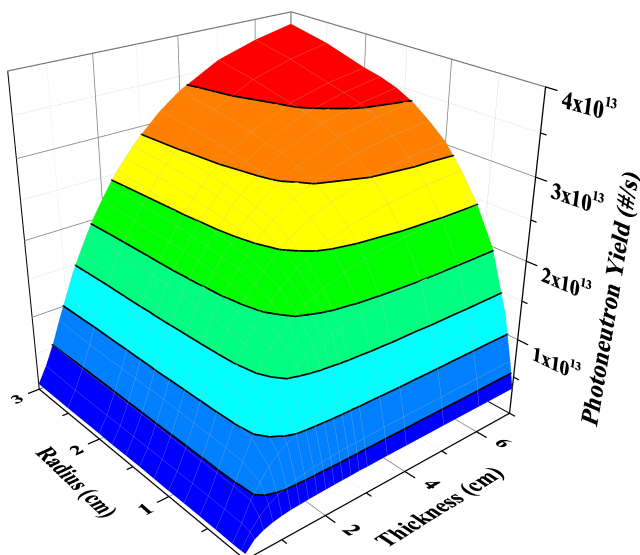


Figure 12: Photon neutron yield (equal to Mo-99 production yield) in cylindrical Mo-100 target.

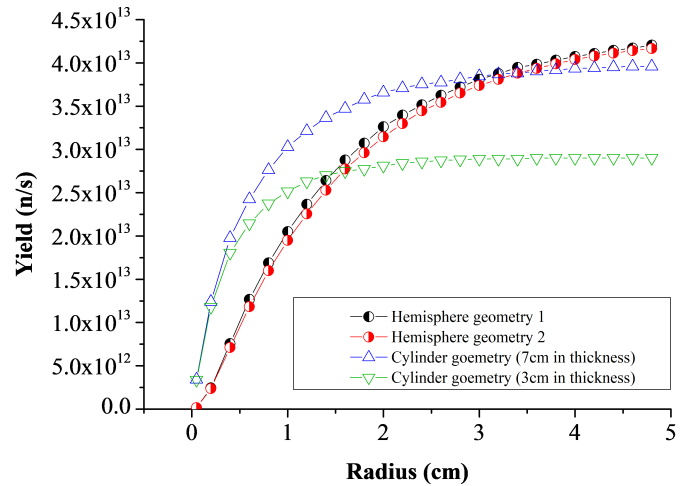


Figure 13: Neutron production yields (which is in correspondent with Mo-99 production yield) for different geometries of one-stage approach.

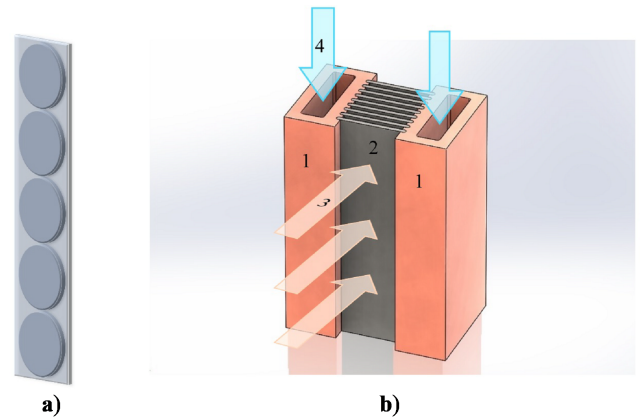


Figure 14: a) Molybdenum discs along each other as a strip target. b) Schematic view of target structure: (1) copper tubes, (2) Mo-100 plates, (3) electron beam direction, (4) water flow direction into the cooling ducts.

The different geometries for copper tube have been studied. The rectangular channel, with large contact area with target has been selected. It should be mentioned that using this type of structure, two-stage approach can be also provided only by replacement of first Molybdenum plate with a tungsten plate.

The basic equation for heat removal by convection is given in Newton’s law of cooling (Bergman et al., 2011):

$$Q = h.A(T_w - T_\infty) \quad (1)$$

where Q is the heat removal rate (W), A is the cross-sectional area (m^2), h is the heat transfer coefficient ($W/m^2.K$), T_w is the object’s surface temperature and T_∞ is the fluid temperature (K). Melting point of molybdenum and copper is 2623 and 1085 °C, respectively. It should be noted that the temperature must be kept low enough to avoid recrystallization of target. Recrystallization happens at 50-70% of the melting point temperature which results cracks, surface roughening, and swelling and also affects the mechanical and thermal properties of the

material (Doherty et al., 1997). So, the reliable temperature of molybdenum target has been considered 1300 °C.

For steady-state thermal analysis, in addition to the power deposition, the heat transfer coefficient can be calculated by the following equation (Bergman et al., 2011):

$$h = \frac{Nu \cdot k}{D} \quad (2)$$

where Nu is the Nusselt number (ratio of convective to conductive heat transfer across the boundary), k is the thermal conductivity ($\text{W}/\text{m}^2 \cdot \text{K}$), and D is the hydraulic diameter (m). The Nusselt number depends on other mechanical dimensionless parameters such as Reynolds and Prandtl numbers (Bergman et al., 2011):

$$Pr = \frac{\nu}{\alpha} = \frac{Cp \cdot \mu}{k} \quad (3)$$

$$Re = \frac{\rho \cdot V \cdot d}{\mu} = \frac{\mu \cdot L}{\nu} \quad (4)$$

where ν is the kinematic viscosity (m^2/s), α is the thermal diffusivity (m^2/s), Cp is the specific heat ($\text{J}/\text{kg} \cdot \text{K}$), ρ is the fluid density (kg/m^3), μ is the dynamic viscosity of the fluid and ($\text{kg}/\text{m} \cdot \text{s}$) and V is the velocity of the fluid (m/s). In this simulation, following Eq. (3), the Prandtl number is fixed on the amount of 6.24. But the Reynolds number, defined by Eq. (4), is the main parameter to determine the flow regime.

Three regimes describe the flow situation (Marhauser, 2006; White and Corfield, 2006):

1. Laminar regime: $Re \leq 2320$
2. Transient regime: $2320 < Re < 10000$
3. Turbulent regime: $Re \geq 10000$

Turbulent flow is a desired regime in which water have more opportunity to contact with surface due to the vortex currents, so the heat transfer rate will increase and leads better cooling process (Bergman et al., 2011; White and Corfield, 2006). Therefore, the equations related to $Re > 10000$ must be used. The following equations have been used in calculation:

if $0.5 < Pr < 2000$, $10000 < Re < 5 \times 10^6$:

$$Nu = \frac{f}{8} \frac{Re \cdot Pr}{1.07 + 12.7 \sqrt{\frac{f}{8}} (Pr^{2/3} - 1)} \quad (5)$$

if $3000 < Re < 5 \times 10^6$:

$$f = \frac{1}{(0.79 \ln(Re) - 1.64)^2} \quad (6)$$

where f is friction factor (generally depends on the surface condition) (White and Corfield, 2006). Table 1 shows the quantity of thermal-mechanical parameters for a rectangular water duct with dimension of 36 mm in length and 10 mm in width (hydraulic diameter, $D_H = 15.65 \times 10^{-3}$ m). It should be noted that the turbulent flow regime can be obtained by choosing the velocities more than 0.6 m/s.

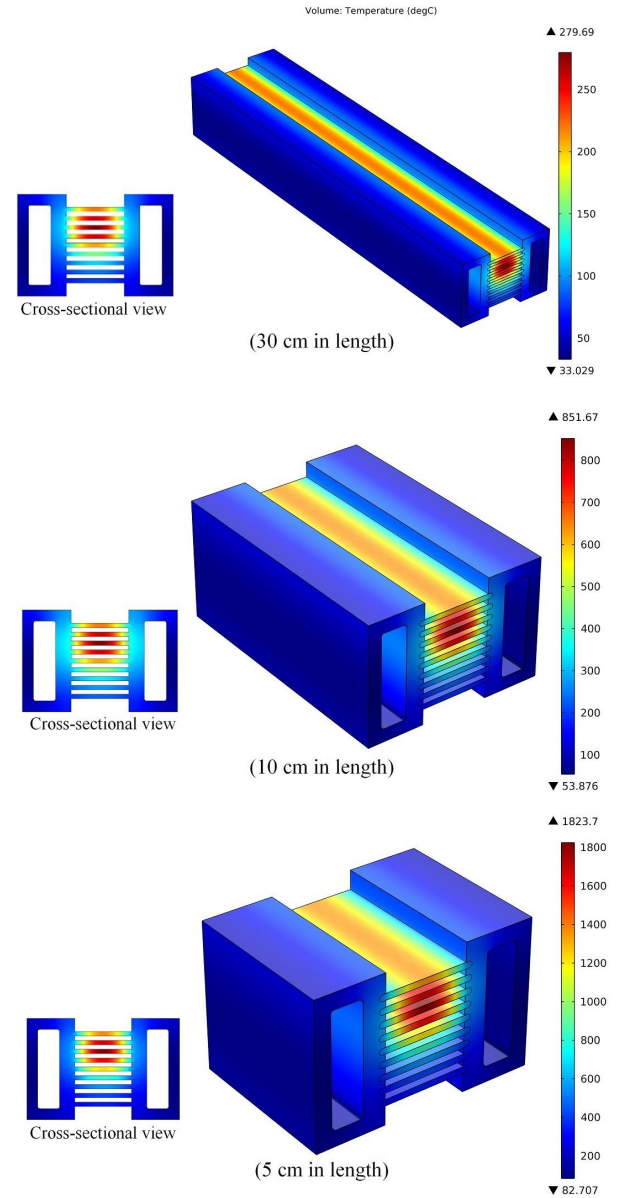


Figure 15: Temperature distribution for strips with different lengths at steady-state mode ($v=2.5$ m/s and $T_\infty=22$ °C).

Table 1: Quantity of thermal-mechanical parameters (V : inlet velocity and Q : Volumetric flow rate) for different velocities of water in tube ($D_H = 15.65 \times 10^{-3}$ m).

V (m/s)	Q (L/min)	Re	Nu	h ($\text{W}/\text{m}^2 \cdot \text{°C}$)
0.6	7.27	10500	80	3332
1	11.54	16750	125	4870
1.5	17.31	25125	177	6850
2	23.08	33500	218	8475
2.5	28.85	41870	276	10700
46.16	46.16	67000	398	15445

The length of target is also an important parameter. By considering the length of beam extraction and electron scanning system (horn) of majority of industrial accelerators as well as the restriction in the target size (expensive raw material, Mo-100), the length of target less than 30 cm has been selected for this study. The deposited energy

Table 2: The deposited energy and power in target.

Mo-100 plates under beam irradiation	Energy deposition in target (MeV)			Power deposition in unit volume of target (10^7 W/m ³)		
	For 5 cm	For 10 cm	For 30 cm	For 5 cm	For 10 cm	For 30 cm
Plate 1	2.967	2.979	2.985	98.893	49.656	16.586
Plate 2	3.689	3.725	3.737	122.963	62.077	20.760
Plate 3	4.025	4.118	4.142	134.172	68.637	23.014
Plate 4	3.540	3.681	3.719	118.006	61.356	20.659
Plate 5	2.501	2.638	2.677	83.362	43.975	14.871
Plate 6	1.477	1.575	1.605	49.219	26.255	8.917
Plate 7	0.798	0.861	0.884	26.620	14.361	4.914
Plate 8	0.47	0.521	0.539	15.816	8.678	2.994
Plate 9	0.338	0.374	0.390	11.253	6.232	2.168

and the power as well as temperature distribution profiles of strips (5, 10, and 30 cm in length) are shown in Table 2 and Fig. 15, respectively. In these calculations, $h = 10700$ W/m².K which is equivalent to fluid velocity of 2.5 m/s. It can be seen that energy deposition is approximately independent from the length of strips, so if the cross section of target is large enough in comparison to electron beam cross section, energy deposition only depends on electron energy and thickness of target.

The effect of coolant velocity has been also investigated in the target. As shown in Fig. 16, temperature variations with velocity more than 2.5 m/s show no significant effect. As seen, for lengths more than 10 cm, the temperature is lower than the mentioned temperature (1300 °C).

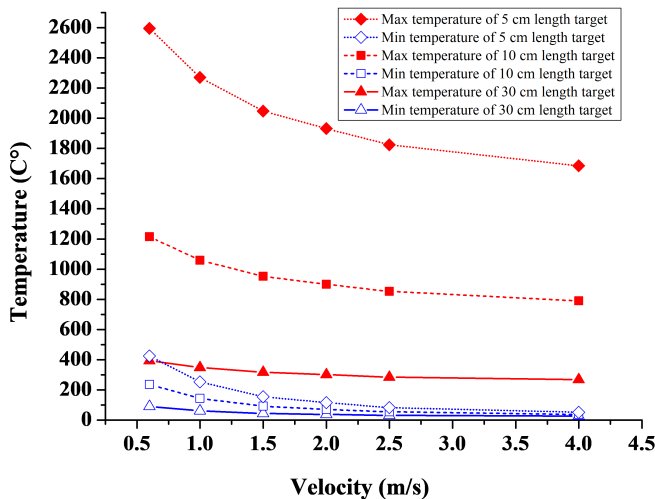


Figure 16: Maximum and minimum temperature of strips with 5, 10, and 30 cm in length according to the different velocities of cooling water.

6 Conclusion

In this work, the optimized nuclear-mechanical design for Mo-99 production target has been presented through photon-neutron interaction $^{100}\text{Mo}(\gamma, n)^{99}\text{Mo}$ based on 30 kW (30 MeV, 1 mA) electron Linac. First, the nuclear calculations have been performed using MCNPX2.6 code to find the best dimensions of target based on the higher Mo-99 production rate, then by considering the construction and

cooling requirements, the molybdenum strips with copper clamps as cooling ducts for water flow have been proposed as a main structure of target. The target assembly contains nine Mo-100 strips with length, width, and thickness equal to 10, 3, and 0.2 cm, respectively (total thickness of 1.8 cm).

Considering 2.5 m/s as an inlet water velocity in the cooling ducts with internal cross section of $3.6 \text{ cm} \times 1 \text{ cm}$, (hydraulic diameter $D = 15.65 \times 10^{-3}$ m), the volumetric flow rate of 28.85 L/min keep the maximum temperature of target assembly less than 900 °C. So, the designed target can be used in one-stage approach in safety condition.

Related calculation on the obtainable activity of each strip and operational tests will be presented in future works. It should be mentioned that using this proposed structure, two-stage approach can be also provided only by replacement of first molybdenum plate with a tungsten plate.

References

- Bennett, R. G., Christian, J. D., Petti, D. A., et al. (1999). A system of ^{99m}Tc production based on distributed electron accelerators and thermal separation. *Nuclear technology*, 126(1):102–121.
- Bergman, T. L., Incropera, F. P., DeWitt, D. P., et al. (2011). *Fundamentals of heat and mass transfer*. John Wiley & Sons.
- Bradley, E. (2013). *Non-HEU production technologies for Molybdenum-99 and Technetium-99m*. International Atomic Energy Agency.
- Brown, D. (2014). Electron linacs: From the laboratory to the factory floor. Technical report, Mevex Corporation, February, CERN: CLIC Workshop.
- COMSOL (2011). COMSOL Multiphysics, Version 4.2, COMSOL. Inc., <http://www.comsol.com>.
- Council, N. R. et al. (2009). *Medical isotope production without highly enriched uranium*. National Academies Press.
- Dale, G., Chemerisov, S., Vandegriff, G., et al. (2010). Global Threat Reduction Initiative (GTRI) Accelerator Production of ^{99}Mo . Technical report, Los Alamos National Laboratory Report LA-UR-11-2010.
- Dale, G. E., Kelsey IV, C. T., Woloshun, K. A., et al. (2012). LANL activities supporting electron accelerator production of ^{99}Mo for NorthStar Medical Radioisotopes, LLC. Technical

report, Los Alamos National Lab.(LANL), Los Alamos, NM (United States).

Diamond, W., Nagarkal, V., REGIER, C., et al. (2017). Production of molybdenum-99 using electron beams. US Patent 9,837,176.

Diamond, W., Nagarkal, V., REGIER, C., et al. (2018). Production of molybdenum-99 using electron beams. US Patent 9,892,808.

Doherty, R., Hughes, D., Humphreys, F., et al. (1997). Current issues in recrystallization: a review. *Materials Science and Engineering: A*, 238(2):219–274.

Esposito, J., Bello, M., Boschi, A., et al. (2013). Accelerator-based alternatives to non-HEU production of Tc-99m. *Final Report of the Coordinated Research Project on Accelerator-Based Alternatives to Non-HEU Production of Mo-99/Tc-99m*, pages 110–119.

Esposito, J., Bello, M., Boschi, A., et al. (2017). Accelerator-based alternatives to non-HEU production of Tc-99m. *Final Report of the Coordinated Research Project on Accelerator-Based Alternatives to Non-HEU Production of Mo-99/Tc-99m*, pages 110–119.

Fedorchenko, D. and Tsechanski, A. (2019). Photoneutronic aspects of the molybdenum-99 production by means of electron linear accelerators. *Nuclear Instruments and Methods in Physics Research Section B: Beam Interactions with Materials and Atoms*, 438:6–13.

Fong, A., Meyer, T., and Zala, K. (2008). Making medical isotopes: report of the task force on alternatives for medical-isotope production. *TRIUMF, Vancouver*.

IAEA (2017). IAEA, Coordinated Research Project (CRP): New Ways of Producing Tc-99m and Tc-99m Generators (Beyond Fission and Cyclotron Methods). <https://www.iaea.org/projects/crp/f22068>.

JANIS (2020a). JANIS Books-proton, online. <http://www.oecd-nea.org/janisweb/book/protons/Mo100/MT16>.

JANIS (2020b). JANIS Books-proton, online. <http://www.oecd-nea.org/janisweb/book/gammas/Mo100/MT4>.

Junior, Joao Alberto Osso and, J. A. (2017). New ways of producing ^{99m}Tc and ^{99m}Tc generators. *Report on the 1st Research Coordination Meeting on New Ways of Producing ^{99m}Tc and ^{99m}Tc Generators*.

Marhauser, F. (2006). Finite element analyses for rf photoinjector gun cavities. Technical report, Deutsches Elektronen-Synchrotron (DESY).

National Academies of Sciences, E., Medicine, et al. (2016). Molybdenum-99 for medical imaging.

Pelowitz, D. B. (2008). MCNPX users manual, version 2.6.0, LA-CP-07-1473. *Los Alamos National Laboratory, Los Alamos (NM)*.

Peykov, P. and Cameron, R. (2014). The Supply of Medical Radioisotopes. Medical Isotope Supply in the Future: Production Capacity and Demand. Forecast for the 99 Mo/99m Tc Market, 2015-2020. Technical report, Organisation for Economic Co-Operation and Development.

Ross, C. and Diamond, W. (2015). Predictions regarding the supply of ^{99}Mo and ^{99m}Tc when NRU ceases production in 2018. *arXiv preprint arXiv:1506.08065*.

Ross, C., Galea, R., Saull, P., et al. (2010). Using the 100 Mo photoneutron reaction to meet Canadas requirement for ^{99m}Tc . *Physics in Canada*, 66(1):24.

Rovais, M. R. A., Aardaneh, K., Aslani, G., et al. (2016). Assessment of the direct cyclotron production of ^{99m}Tc : An approach to crisis management of ^{99m}Tc shortage. *Applied Radiation and Isotopes*, 112:55–61.

Torabi, F., Masoudi, S. F., and Rahmani, F. (2013). Photoneutron production by a 25 MeV electron linac for BNCT application. *Annals of Nuclear Energy*, 54:192–196.

Tsechanski, A., Bielajew, A., Archambault, J., et al. (2016). Electron accelerator-based production of molybdenum-99: Bremsstrahlung and photoneutron generation from molybdenum vs. tungsten. *Nuclear Instruments and Methods in Physics Research Section B: Beam Interactions with Materials and Atoms*, 366:124–139.

White, F. M. and Corfield, I. (2006). *Viscous fluid flow*, volume 3. McGraw-Hill New York.